

ChemComm

Chemical Communications

Accepted Manuscript

This article can be cited before page numbers have been issued, to do this please use: X. Wang, K. Li, H. Xu, N. Ali, Y. Wang, Q. Shen and H. Wu, *Chem. Commun.*, 2020, DOI: 10.1039/D0CC01847C.



This is an Accepted Manuscript, which has been through the Royal Society of Chemistry peer review process and has been accepted for publication.

Accepted Manuscripts are published online shortly after acceptance, before technical editing, formatting and proof reading. Using this free service, authors can make their results available to the community, in citable form, before we publish the edited article. We will replace this Accepted Manuscript with the edited and formatted Advance Article as soon as it is available.

You can find more information about Accepted Manuscripts in the [Information for Authors](#).

Please note that technical editing may introduce minor changes to the text and/or graphics, which may alter content. The journal's standard [Terms & Conditions](#) and the [Ethical guidelines](#) still apply. In no event shall the Royal Society of Chemistry be held responsible for any errors or omissions in this Accepted Manuscript or any consequences arising from the use of any information it contains.

COMMUNICATION

Synthesis of Large Two-Dimensional Lead-Free Bismuth-Silver Double Perovskites Microplatelets and Application for Field-Effect Transistors

Received 00th January 20xx,
Accepted 00th January 20xx

Xiaoyu Wang, Kai Li, Hanlun Xu, Nasir Ali, Yao Wang, Qibin Shen and Huizhen Wu*

DOI: 10.1039/x0xx00000x

Two-dimensional phenylethylammonium (PEA, $C_8H_9NH_3$) Bi-Ag double perovskites $(PEA)_4BiAgX_8$ ($X=Br, I$) microplatelets are synthesized for the first time via a facile self-assembly recrystallization method. Absorption of microplatelets exhibit direct bandgaps and different halide compositions show distinct morphologies and bandgap tunability. Field-effect transistors based on single $(PEA)_4BiAgBr_8$ microplatelet display a p-type semiconducting behavior.

Owing to their peculiar optoelectronic properties and facile solution processability, organo-lead halide perovskites (PVKs) have been extensively utilized for varieties of optoelectronic applications, such as photovoltaics, light-emitting diodes, and photodetectors, etc.¹⁻³. Nevertheless, the bioaccumulation of their major component (lead) compelled the researchers to focus on other lead-free alternatives of halide PVKs materials. In this regard, several homovalent and heterovalent substitutes have been introduced.⁴ Among these substitutes, Sn^{2+} suffered from rapid oxidation to its stable Sn^{4+} state. Similarly, Bi^{3+} -based PVKs exhibited better environmental stability with poor photovoltaic performance duo to their lower deminsionality.^{5,6}

To cope with this issue, a new class of lead-free PVKs, i.e., double PVKs with general formula $A_2MM'X_6$ have been introduced,⁷ where M is a monovalent cation (e.g., Na^+ , Ag^+ , etc.) and M' is a trivalent cation (e.g., Bi^{3+} , Sb^{3+} , etc.). The two Pb^{2+} cations are substituted with one monovalent and one trivalent cation to retain the structure dimensionality. Among various double PVKs, A_2BiAgX_6 has successfully utilized in X-ray detectors⁸ and solar cells⁹. Although, less toxic Ag^+ and Bi^{3+} have completely replaced the toxic Pb^{2+} . Unfortunately, due to their intrinsic indirect bandgap,¹⁰ it could not compete with Pb^{2+} based PVKs materials. However, recently it has been reported that by reducing the dimension of Bi-Ag double PVKs into 2D, the bandgap can be switched into a direct one.¹¹ Subsequently,

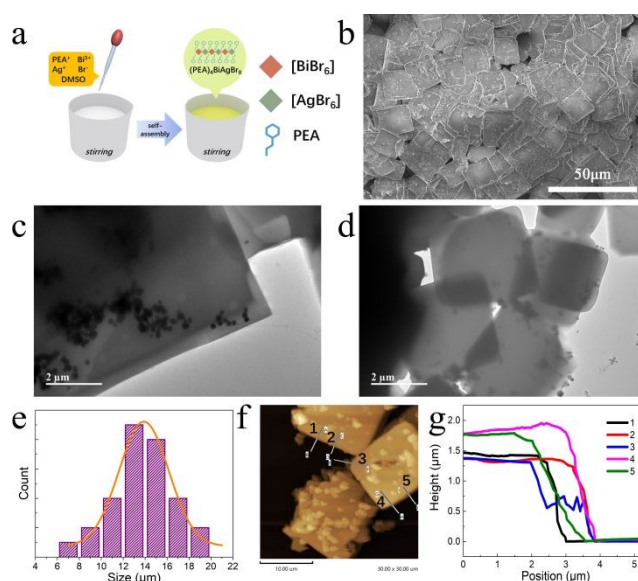


Figure 1. (a) A schematic diagram of the recrystallization method, where PEA induces the lateral crystallization of $(PEA)_4BiAgBr_8$ MPs. (b) SEM image of the $(PEA)_4BiAgBr_8$ MPs and (c, d) are their TEM images. (e) A histogram of the lateral size distribution of the $(PEA)_4BiAgBr_8$ MPs. (f) SPM image of the $(PEA)_4BiAgBr_8$ MPs and (g) are their thickness measurement.

direct bandgap 2D Bi-Ag double PVKs single crystals and thin films were fabricated.¹² These were promising studies to utilize Bi-Ag double PVKs as a non-toxic alternative to the lead-based PVKs. Therefore, we endeavored on finding a facile way to synthesize 2D Bi-Ag double PVKs and verifying its direct bandgap property from its optical characteristics.

In this work, we successfully synthesized free-standing 2D halide double PVKs $(PEA)_4BiAgBr_8$ microplatelets (MPs) for the first time via a facile self-assembly anti-solvent recrystallization method (ASRC) in ambient conditions. This method was previously employed both for nanocrystals (NCs) and nanosheets (NSs) synthesis.^{13,14} Typically, the ASRC involves the injection into a suitable solvent with a relatively poor solubility of the precursor solutes, triggering fast self-assembly recrystallization, as schematized in **Figure 1a**. Here, dimethyl sulfoxide (DMSO) is used as a precursor solvent and chloroform ($CHCl_3$) as the recrystallization solvent to obtain ultra-large high-quality 2D $(PEA)_4BiAgBr_8$ MPs. Since we used a long-chain

Department of Physics and State Key Laboratory for Silicon Materials, Zhejiang University, Hangzhou, China. E-mail: hzwu@zju.edu.cn

Electronic Supplementary Information (ESI) available: [details of any supplementary information available should be included here]. See DOI: 10.1039/x0xx00000x

organic cation, i.e., PEA⁺ instead of Cs⁺ or MA⁺; therefore, the growth of the crystals is restricted to form a 2D structure. Conversely, the conventional A sites could only result in nanocrystals.¹⁵ Compared with the previous reported single crystal growth of 2D Bi-Ag double PVKs, which need to be kept at 100°C for 60 h,¹² this method is less energy and consumptions.

Firstly, the structural and morphological characteristics of the prepared (PEA)₄BiAgBr₈ MPs were studied. A comparatively optical absorbance revealed a direct bandgap of the MPs. Furthermore, 2D Bi-Ag double PVKs with different halide compositions were also synthesized, which not only exhibited distinct morphologies but also tunable bandgaps. To demonstrate the application of the prepared MPs, a single (PEA)₄BiAgBr₈ MP was utilized to fabricate a FET through a dry-transfer procedure. Up to the best of our knowledge, this is the first colloidal synthesis of the free-standing 2D Bi-Ag double PVKs with ultra-large lateral size and their utilization in FETs. Due to their free-standing nature in colloidal form, the MPs could easily be utilized in a variety of optoelectronic applications.

Figure 1b shows the scanning electron microscopy (SEM) image of as-synthesized (PEA)₄BiAgBr₈ MPs. Square-shaped with larger size MPs were obtained using chloroform, comparable with the 2D PVKs obtained via chemical vapor deposition (CVD) technique.^{16, 17} Multiple nanoparticles adhered on the surface of MPs may be the by-products, i.e., BiBr₃, AgBr, and (PEA)₃Br₂Br₉, etc. The rapid-recrystallization process could be the reason of leftover products. The average size of the MPs was estimated to be 13.75 μm. For size distribution histogram, see **Figure 1e**, which is significantly larger than other 2D halide PVKs obtained via the other similar same routes.^{14, 18} Larger sized MPs could easily be observed under an optical microscope, showing its feasibility for device employment. Furthermore, it is revealed from the energy dispersive spectroscopy (EDS) results that (PEA)₄BiAgBr₈ MPs exhibit a homogeneous distribution of the constituent elements as shown in **Figure S1**. Transmission electron microscopy (TEM) images showed that MPs have rectangular structures with sharp edges, see **Figure 1c** and **1d**. Similarly, the thickness and surface roughness were studied by scanning probe microscopy (SPM), as shown in **Figure 1f**. In accordance with SEM and TEM analyses, multiple nanoparticles adhered to the MPs were observed. In comparison with the surface of the substrate, the height profile of the single MP was measured to be 1.25-1.75 μm, as depicted in **Figure 1g**. Because of nanoparticles attached both sides, we deduced that the actual thickness of single MP may be smaller than measured results. Additionally, the surface roughness analysis revealed root-mean-square deviations (Rq) of 19.007 nm and 35.564 nm for two 1 μm² squares without any nanoparticles attached, see **Figure S2**. Oleic acid was also employed as a ligand during MPs synthesis but with the SEM image shown in **Figure S3**, no influence from ligand was observed. All the above characterizations were performed for the MPs fabricated in chloroform as a recrystallization solvent. To study the influence of the recrystallization solvent on the (PEA)₄BiAgBr₈ MPs, dichloromethane (CH₂Cl₂) and

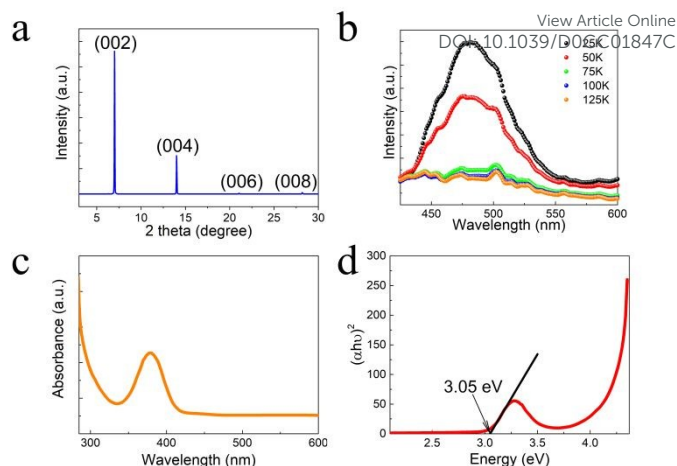


Figure 2. (a) XRD pattern of (PEA)₄BiAgBr₈ MPs. (b) PL spectra of the (PEA)₄BiAgBr₈ MPs at variable temperatures. (c) Absorbance spectrum of (PEA)₄BiAgBr₈ MPs. (d) Tauc plot of the absorbance spectrum of (PEA)₄BiAgBr₈ MPs showing a direct bandgap characteristic.

chlorobenzene (C₆H₅Cl) were utilized to substitute chloroform. Unfortunately, no sheets- or platelets-like products were observed; instead, nanospheres- like morphology was observed (**Figure S4**), which are fragile under the beams of an electron microscope. Their absorbance was also measured and shown in **Figure S5**. It is speculated from the absorbance spectra, that the product composition by dichloromethane is closer to MPs than that by chlorobenzene. We aim is to obtain 2D PVKs for further applications but dichloromethane and chlorobenzene are not suitable. The impact of recrystallization solvents may be due to the difference in the functional groups and solubilities. Different solubilities of each precursor will cause defects, even damage the Bi/Ag chemical ratio, hindering the synthesis of MPs. A further detailed study is required to know the exact reason why some recrystallization solvents are suitable for the fabrication of MPs, as well as a effective method to modify lateral size. Hitherto, chloroform is found to be a suitable recrystallization solvent; therefore, all further characterizations and device fabrication will be based on MPs obtained from chloroform as a recrystallization solvent and other solvents are ruled out.

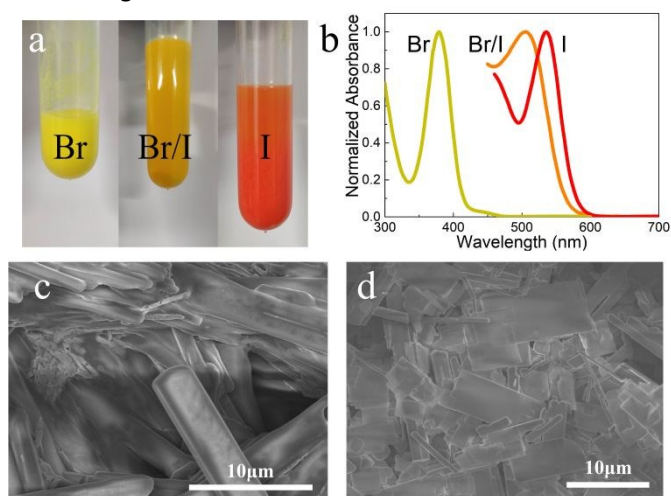
To study the crystallinity of the prepared (PEA)₄BiAgBr₈ MPs, X-ray diffraction (XRD) analysis was carried out, as depicted in **Figure 2a**. The XRD patterns of (PEA)₄BiAgBr₈ MPs show intense and sharp diffraction peaks at 7.0 and 14.0 two theta degree, reflected from (002) and (004) crystal planes, respectively. Besides, two faint diffraction peaks from (006) and (008) crystal planes were also observed. No other impurity peak was observed, indicating the phase purity of the MPs. Smaller full-width-at half-maximum (FWHM) of (002) and (004) plane peaks, i.e., 0.0635 and 0.0664 two theta degree (**Figure S6**), indicates the larger size as well as better crystallinity of the MPs, which is beneficial to electron transportation. The spacing is 7.0 two theta degree and according to Bragg's law, the calculated out-of-plane distance is 1.26 nm, similar to (PEA)₄PbBr₄ PVK nanosheets.¹⁹

Stability test of (PEA)₄BiAgBr₈ MPs was done in the ambient conditions for two weeks aged samples (**Figure S7**). Negligible

variation was observed in the XRD patterns. The two dominant diffraction peaks (002) and (004) were perfectly maintained with rather small FWHMs, indicating better environmental stability of MPs. The enhanced stability is ascribed to the hydrophobic long-chain organic cations at A sites.

Additionally, Raman measurement was also carried out for (PEA)₄BiAgBr₈ MPs. As **Figure S8** shown, the Raman spectrum exhibits three characteristic peaks at 67.91, 137.38 and 157.93 cm⁻¹. These peaks were mainly generated from Bi-Br part of the double PVK, which are obviously different from the pure BiBr₃.²⁰ Therefore, it can be inferred that the Raman signals are originated from the (PEA)₄BiAgBr₈, indicating the absence of stoichiometric residuals.

Likewise, the optical absorption spectrum of (PEA)₄BiAgBr₈ MPs presented in **Figure 2c** shows a sharp absorption edge at 420 nm with an absorption peak at 379 nm without any absorption tail in the lower energy region. Tauc plot of a direct transition shows an ideal result with a standard linear region indicating a direct bandgap of 3.05 eV, and a straighter line below 3.0 eV (**Figure 2d**). Cs₂BiAgBr₆ single crystals (SCs) exhibit an indirect bandgap of 1.95 eV with assisting phonon energy of 0.12 eV,¹⁰ where Cs₂BiAgBr₆ NCs exhibit an indirect bandgap of 2.52 eV.²¹ The bandgap of (PEA)₄BiAgBr₈ is much wider than that of Cs₂BiAgBr₆ SCs and NCs, attributed to the 2D characteristic of MPs.²² A Tauc plot of an indirect bandgap of the absorbance spectrum of (PEA)₄BiAgBr₈ MPs is shown in **Figure S9**. The results are in line with typical direct bandgap PVKs, e.g., MAPbX₃ (X=Cl, Br, and I) single crystals²³ even (PEA)₄BiAgBr₈ MPs share the same M and M' sites component as Cs₂BiAgBr₆. Furthermore, a strong photoluminescence (PL) peak at 481 nm of the MPs was observed at a low temperature (25K) excited by a 404.6 nm laser, and intensity reduced distinctly with the increase of the temperature. There is no obvious PL peak at 75K and above temperature. Due to strong intrinsic quantum confinement in 2D (PEA)₄BiAgBr₈ MPs, excited carriers become bound excitons and relax back to self-trapped states easily, and detrapped by thermal activation, which brings the radiative transition down.²⁴



In order to study the bandgap tunability of the MPs, (PEA)₄BiAgX₈ (X=Br, I) PVKs with different halides were also

Figure 3. (a) Pictures of colloidal solution of (PEA)₄BiAgBr₈, (PEA)₄BiAgBr₄I₄ and (PEA)₄BiAgI₈. (b) Normalized absorbance spectra of MPs with different halide compositions. (c, d) SEM images of (PEA)₄BiAgBr₄I₄ and (PEA)₄BiAgI₈.

synthesized via same method. Upon changing the precursor solutions, we altered the halogen anion from Br to I to synthesize 2D (PEA)₄BiAgBr₄I₄ and (PEA)₄BiAgI₈. **Figure 3a** presents a distinct color change (starting from bright yellow to orange and scarlet) with the increasing ratio of I. The absorption edge of (PEA)₄BiAgBr₈, (PEA)₄BiAgBr₄I₄, and (PEA)₄BiAgI₈ MPs are found to be respectively 412 nm, 561 nm, and 576nm, indicating an obvious red-shift (**Figure 3b**). It is worth noting that 2D Bi-Ag double PVKs with all halide compositions don't show any absorption tail. Tauc plots of direct bandgaps of (PEA)₄BiAgBr₄I₄ and (PEA)₄BiAgI₈ presented in **Figure S10** indicate a bandgap of 2.26 eV and 2.19 eV, respectively. Furthermore, SEM presented significant morphological differences of products with different halide compositions: (PEA)₄BiAgBr₄I₄ have uniform rod-shaped morphology with a large length to width ratio (**Figure 3c**), where (PEA)₄BiAgBr₄I₄ exhibited belt-shapes with a few microrods observed (**Figure 3d**). Beside their different morphologies, these compositions exhibited poor uniformity of morphology in comparison with the (PEA)₄BiAgBr₈ MPs. However, the crystal size of all three compositions was found to be in the micrometer range sizes. As **Figure S11** shown, EDS mapping results demonstrate uniform distributions of metal cations and halide anions of Br and I in each sample. The morphological and optical characteristics of 2D Bi-Ag double PVKs with different halide compositions are listed in **Table S1**. Halide compositions of 2D Bi-Ag double PVKs indeed influence the bandgaps and morphologies, which may facilitate further research and enlarge their application areas.

The intrinsic 2D nature of the solution-processed (PEA)₄BiAgBr₈ MPs restricts the carrier transport laterally.²⁵

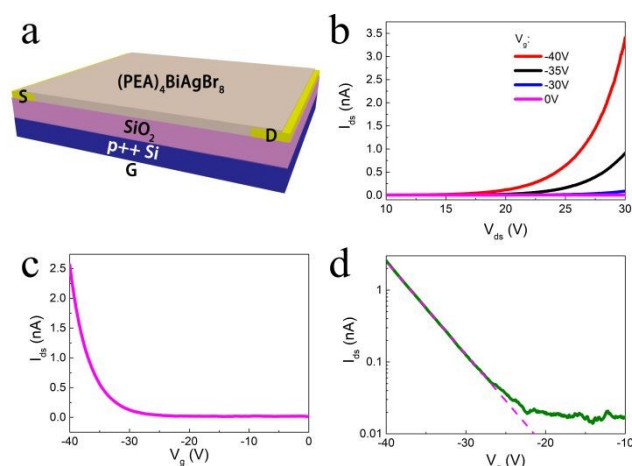


Figure 4. (a) Configuration diagram of (PEA)₄BiAgBr₈ MPs FET. (b) Output characteristic of (PEA)₄BiAgBr₈ MP FET. (c) Transfer characteristic of (PEA)₄BiAgBr₈ MP FET ($V_{ds}=30V$). (d) Transfer characteristic of (PEA)₄BiAgBr₈ MP FET in semi-log plot.

Subsequently, a single (PEA)₄BiAgBr₈ MP was employed to fabricate a FET, as schematized in **Figure 4a**. The optical image was shown in **Figure S12**. The conventional Pb²⁺ based PVKs, as well as the lead-free Sn²⁺ based PVKs have been successfully exploited for FETs application.²⁶ However, to the best of our knowledge, there is no report about FET application based on halide double PVKs. Therefore, employing (PEA)₄BiAgBr₈ MP

into the FET devices is of significant importance. Briefly, we adopted a dry transfer technique in which a single (PEA)₄BiAgBr₈ MP was transferred on the pre-patterned electrodes on SiO₂/Si substrates.¹⁷ The SiO₂ acted as a dielectric layer while a single (PEA)₄BiAgBr₈ MP acted as a channel material. **Figure 4b** and **4c** shows the output characteristics (drain-source current I_{ds} versus drain-source voltage V_{ds}) and transfer characteristics (drain-source current I_{ds} versus gate voltage V_g) of the fabricated (PEA)₄BiAgBr₈ MP FET device. The device displayed a p-type semiconducting behavior as I_{ds} increases when V_g decreases. The device demonstrated the ON/OFF ratio above 100 counts, which can be observed in the semi-log plot of its transfer characteristic (**Figure 4d**). Moreover, the field-effect mobility of a FET was estimated based on the equation¹⁷ $\mu = \frac{L}{WC} \frac{dI_{ds}}{dV_g dV_{ds}}$, where L is the channel length (2 μm), W is the channel width (15 μm), C is the capacitance of the 100 nm SiO₂ layer (3.45 × 10⁻⁶ F/m²) and $V_{ds}=30V$. $\frac{\partial I_{ds}}{\partial V_g}$ can be calculated by fitting the linear region of the curve of I_{ds} versus V_g . The estimated field-effect mobility is about 1.66 × 10⁻⁵ cm²V⁻¹s⁻¹. Considering the MPs were obtained via an anti-solvent recrystallization method, in which the crystallization finishes immediately, numerous defects could be involved inside; therefore, we inferred that defect scattering is one of the main reasons impacting the material mobility. Considering different defect formation energies of vacancies and antisites, modifying the chemical conditions, e.g., offering a Bi- or Ag-rich condition, is one of the promising methods improving mobility.²⁷

In summary, we successfully synthesized high-quality large 2D lead-free Bi-Ag double PVKs (PEA)₂BiAgBr₈ MPs via a facile self-assembly ASRC method for the first time. By a series of optical characterizations and comparison with reported PVKs, we estimated that (PEA)₂BiAgBr₈ MPs have a direct bandgap, which is in line with the previous reports. An ideal Tauc plot of direct bandgap indicated a bandgap of 3.05 eV. We also altered the halide compositions, and fabricated (PEA)₄BiAgBr₄I₄ and (PEA)₄BiAgI₈, which showed distinct morphologies and bandgap shrinkage. Finally, a single (PEA)₂BiAgBr₈ MP was utilized to fabricate a FET device via a dry transfer technique. The device demonstrated satisfactory performance, i.e., transfer characteristics and ON/OFF ratio. Since the (PEA)₂BiAgBr₈ MPs are easy to prepare in a colloidal form and transfer on any type of substrates; therefore, we believe that this work will provide a better guideline to the development and applications of lead-free double PVKs.

This work was supported by the National Natural Science Foundation of China (Grant No. U1737109 and 1193306).

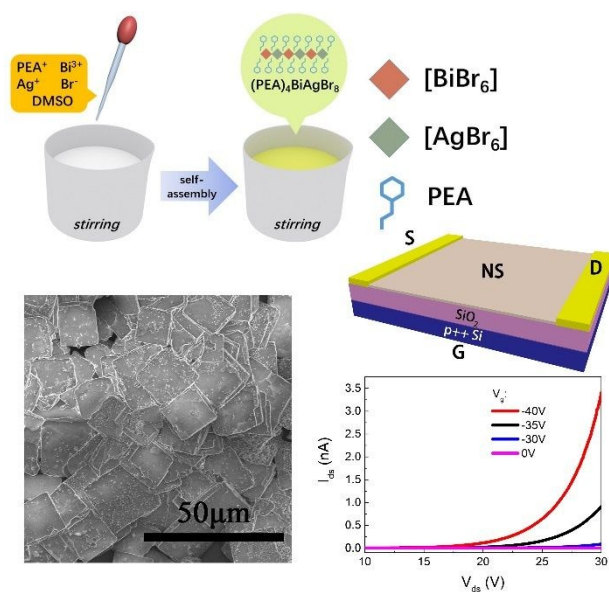
Conflicts of interest

There are no conflicts to declare.

Notes and references

1. F. Sahli, J. Werner, B. A. Kamino, M. Bräuninger, R. Monnard, B. Paviet-Salomon, L. Barraud, L. Ding, J. J. Diaz Leon, D. Sacchetto, G. Cattaneo, M. Despeisse, M. Boccard, S. Nicolay, Q. Jeangros, B. Niesen and C. Ballif, *Nature Materials*, 2018, **17**, 820-826.
2. H. Cho, Y.-H. Kim, C. Wolf, H.-D. Lee and T.-W. Lee, *Advanced Materials*, 2018, **30**, 1704587.
3. Z. Yang, Y. Deng, X. Zhang, S. Wang, H. Chen, S. Yang, J. Khurgin, N. X. Fang, X. Zhang and R. Ma, *Advanced Materials*, 2018, **30**, 1704333.
4. S. Chatterjee and A. J. Pal, *Journal of Materials Chemistry A*, 2018, **6**, 3793-3823.
5. B. Wu, Y. Zhou, G. Xing, Q. Xu, H. F. Garces, A. Solanki, T. W. Goh, N. P. Padture and T. C. Sum, *Advanced Functional Materials*, 2017, **27**.
6. B. Ghosh, B. Wu, H. K. Mulmudi, C. Guet, K. Weber, T. C. Sum, S. Mhaisalkar and N. Mathews, *ACS Appl Mater Interfaces*, 2018, **10**, 35000-35007.
7. L. Liang and P. Gao, *Advanced Science*, 2018, **5**.
8. W. Pan, H. Wu, J. Luo, Z. Deng, C. Ge, C. Chen, X. Jiang, W.-J. Yin, G. Niu, L. Zhu, L. Yin, Y. Zhou, Q. Xie, X. Ke, M. Sui and J. Tang, *Nature Photonics*, 2017, **11**, 726-732.
9. W. Gao, C. Ran, J. Xi, B. Jiao, W. Zhang, M. Wu, X. Hou and Z. Wu, *Chemphyschem*, 2018, **19**, 1696-1700.
10. A. H. Slavney, T. Hu, A. M. Lindenberg and H. I. Karunadasa, *J Am Chem Soc*, 2016, **138**, 2138-2141.
11. B. A. Connor, L. Leppert, M. D. Smith, J. B. Neaton and H. I. Karunadasa, *J Am Chem Soc*, 2018, **140**, 5235-5240.
12. M. K. Jana, S. M. Janke, D. J. Dirkes, S. Dovletgeldi, C. Liu, X. Qin, K. Gundogdu, W. You, V. Blum and D. B. Mitzi, *Journal of the American Chemical Society*, 2019, DOI: 10.1021/jacs.9b02909.
13. F. Zhang, H. Zhong, C. Chen, X.-g. Wu, X. Hu, H. Huang, J. Han, B. Zou and Y. Dong, *ACS Nano*, 2015, **9**, 4533-4542.
14. S. Yang, W. Niu, A. L. Wang, Z. Fan, B. Chen, C. Tan, Q. Lu and H. Zhang, *Angew Chem Int Ed Engl*, 2017, **56**, 4252-4255.
15. B. Yang, J. Chen, S. Yang, F. Hong, L. Sun, P. Han, T. Pullerits, W. Deng and K. Han, *Angew Chem Int Ed Engl*, 2018, **57**, 5359-5363.
16. Y. Wang, Y. Shi, G. Xin, J. Lian and J. Shi, *Crystal Growth & Design*, 2015, **15**, 4741-4749.
17. C. Huo, X. Liu, X. Song, Z. Wang and H. Zeng, *J Phys Chem Lett*, 2017, **8**, 4785-4792.
18. W. Deng, X. Jin, Y. Lv, X. Zhang, X. Zhang and J. Jie, *Advanced Functional Materials*, 2019, **29**.
19. R. Guo, Z. Zhu, A. Boulesbaa, F. Hao, A. Puzetzy, K. Xiao, J. Bao, Y. Yao and W. Li, *Small Methods*, 2017, **1**.
20. R. P. Oertel and R. A. Plane, *Inorganic Chemistry*, 1969, **8**, 1188-1190.
21. L. Zhou, Y. F. Xu, B. X. Chen, D. B. Kuang and C. Y. Su, *Small*, 2018, **14**, e1703762.
22. N. Ali, S. Rauf, W. Kong, S. Ali, X. Wang, A. Khesro, C. P. Yang, B. Zhu and H. Wu, *Renewable and Sustainable Energy Reviews*, 2019, **109**, 160-186.
23. Y. Liu, Z. Yang, D. Cui, X. Ren, J. Sun, X. Liu, J. Zhang, Q. Wei, H. Fan, F. Yu, X. Zhang, C. Zhao and S. F. Liu, *Adv Mater*, 2015, **27**, 5176-5183.
24. Y. Fang, L. Zhang, L. Wu, J. Yan, Y. Lin, K. Wang, W. L. Mao and B. Zou, *Angewandte Chemie*, 2019, **131**, 15393-15397.
25. M. K. Li, T. P. Chen, Y. F. Lin, C. M. Raghavan, W. L. Chen, S. H. Yang, R. Sankar, C. W. Luo, Y. M. Chang and C. W. Chen, *Small*, 2018, **14**, e1803763.
26. T. Matsushima, S. Hwang, A. S. Sandanayaka, C. Qin, S. Terakawa, T. Fujihara, M. Yahiro and C. Adachi, *Adv Mater*, 2016, **28**, 10275-10281.
27. Z. Xiao, W. Meng, J. Wang and Y. Yan, *ChemSusChem*, 2016, **9**, 2628-2633.

Table of Contents

View Article Online
DOI: 10.1039/D0CC01847C

Two-dimensional double perovskite $(\text{PEA})_4\text{BiAgX}_8$ microplatelets are synthesized for the first time with application in field-effect transistors.